Journal of Power Sources 196 (2011) 6131–6137

Contents lists available at ScienceDirect

Journal of Power Sources

journal homepage: www.elsevier.com/locate/jpowsour

Effect of zinc oxide doping on the grain boundary conductivity of $Ce_{0.8}Ln_{0.2}O_{1.9}$ ceramics (Ln = Y, Sm, Gd)

Lin Ge, Shujun Li, Yifeng Zheng, Ming Zhou, Han Chen, Lucun Guo*

College of Materials Science and Engineering, Nanjing University of Technology, No. 5 Xinmofan Road, Nanjing, Jiangsu 210009, PR China

ARTICLE INFO

Article history:
Received 28 January 2011
Received in revised form 13 March 2011
Accepted 15 March 2011
Available online 23 March 2011

Keywords:
Solid oxide fuel cell
Doped ceria
Zinc oxide
Sintering aid
Grain-boundary conduction

ABSTRACT

The effect of zinc oxide (ZnO) doping on the densification behaviours and the electrical properties of $Ce_{0.8}Ln_{0.2}O_{1.9}$ (Ln = Y, Sm, Gd) ceramics are examined. The addition of ZnO (1 mol%) reduces the sintering temperature by ~200 °C and improves the grain boundary behaviours significantly. Both the apparent grain boundary conductivity (σ_{gb}^{app}) and the specific grain boundary conductivity (σ_{gb}^{sp}) are investigated. Under the same synthetic conditions, ZnO doping leads to a larger grain size and a higher σ_{gb}^{sp}. The SEM and EDS results indicate that ZnO-doping can induce Si enrichment on the surfaces of samples (i.e. reducing the content of Si at grain boundaries), which may explain the improvements occurs in the grain boundary conductions.

1. Introduction

In recent years, due to the higher ionic conductivity and lower interfacial losses with electrode, doped ceria has attracted great attention as a type of promising electrolyte for intermediate temperature (500–800 °C) SOFC (IT-SOFC) [1–3]. Partial substitution of tetravalent Ce^{4+} by rare-earth or alkaline-earth additives (Ca^{2+}, Y^{3+}, La^{3+}, Gd^{3+}, Sm^{3+}, Sc^{3+}, Sr^{2+}) was found to be effective in enhancing the ionic conductivity and hindering the reducibility under low oxygen partial pressure [3–10]. Y^{3+}, Sm^{3+} and Gd^{3+} doped ceria are considered to be the potentially most useful electrolytes because of their relatively high ionic conductivities [5–8].

In low and intermediate temperature regions, the contribution of grain boundary resistivity to the overall resistivity is significant [11]. The specific grain-boundary resistivity was reported to be ~10^2–10^5 times higher than the grain-interior resistivity [12,13]. In ceria-based electrolyte materials, small amount of impurities are inadvertently incorporated in the starting ceramic powders during manufacturing process and tend to accumulate at grain boundaries [14,15]. These impurities such as Si and Ca segregate at grain boundaries and form amorphous layers, which block charge carriers and consequently lead to higher grain boundary resistivity [15–17]. Besides precipitation of amorphous phases, other problems, such as mismatch of the lattices, microcracks, solute segregation and space charge in the vicinity of the grain boundaries can all result in a highly resistive grain boundary phase [18].

On the other hand, one of the main problems in ceria-based materials is poor sinterability. For the sintering aid, Co_2O_3, CuO and MnO_2 have been reported effectively improving the densification but they show detrimental influence on the grain boundary conductivity [7,19–23]. Fe_2O_3 and MgO were reported to be not only good sintering aids but also scavengers of SiO_2 impurity in the ceria-based electrolytes [22,23]. Recently, ZnO was found to be an effective sintering aid for YDC [7,8]. However, there is still a lack of systematic studies reported on the influence of ZnO doping on the grain boundary behaviour.

The aim of this study is to investigate the effect of ZnO on the grain interior and grain boundary behaviours of $Ce_{0.8}Ln_{0.2}O_{1.9}$ (Ln = Y, Sm, Gd) (20YDC, 20SDC, 20GDC). Special attention is paid to the variation of the grain boundary conductivity.

2. Experimental

2.1. Sample preparation

Commercial rare earth powders were used in this study (Table 1). Powders of $Ce_{0.8}Y_{0.2}O_{1.9}$ (20YDC), $Ce_{0.8}Sm_{0.2}O_{1.9}$ (20SDC) and $Ce_{0.8}Gd_{0.2}O_{1.9}$ (20GDC) were first prepared by the solid state reaction process. Stoichiometric quantities of CeO_2–Y_2O_3, CeO_2–Sm_2O_3 and CeO_2–Gd_2O_3 powders were mixed with distilled water for 8 h, using zirconia balls as milling media in a planetary mill. After being dried and ground, the powders were calcined in air at 1200 °C for 2 h. X-ray fluorescence (XRF) analysis of the

* Corresponding author. Tel.: +86 25 83587261; fax: +86 025 83306152.
E-mail address: lc-guo@163.com (L. Guo).

0378-7753/$ – see front matter © 2011 Elsevier B.V. All rights reserved.
doi:10.1016/j.jpowsour.2011.03.032

Table 1
Sources and purities of raw materials.

Material	Purity (%)	Supplier
CeO_2	99.99	Yixing Xinwei Leeshing Rare Earth Co., Ltd., China
Y_2O_3	99.99	Yixing Xinwei Leeshing Rare Earth Co., Ltd., China
Sm_2O_3	99.95	Beijing Founde Star Science and Technology Co., Ltd., China
Gd_2O_3	99.99	Beijing Founde Star Science and Technology Co., Ltd., China
ZnO	99.95	Shanghai Chemical Reagent Plant, China

calcined 20LnDC powders indicated that the content of SiO_2 was 200–300 ppm and that of CaO was 150–200 ppm. Parts of the calcined 20LnDC powders were, respectively, mixed with zinc oxide in quantities corresponding to 1 mol%. The undoped and ZnO-doped 20LnDC powders were ball-milled together for 8 h and then dried. The obtained powders were ground and axially die pressed into cylindrical pellets (14 mm in diameter) under a pressure of about 100 MPa. Finally the green bodies were sintered in air at 1400–1600 °C for 10 h. Herein, for simplicity, the sintered specimens are denoted as "20LnDC1Zn" and "20LnDC" for $Ce_{0.8}Ln_{0.2}O_{1.9}$ (Ln = Y, Sm, Gd) with and without 1 mol% ZnO additive. For example, a 20SDC1Zn specimen is a 1 mol% ZnO-doped $Ce_{0.8}Sm_{0.2}O_{1.9}$ specimen.

2.2. Characterization

The densities of the sintered pellets were measured using the Archimedes' method in a water bath. Crystal structures were identified by an X-ray diffractometer (XRD, D/max-III, Rigaku) with Cu Kα radiation in the 2θ range of 20–80°. The surfaces of sintered samples were observed using a scanning electron microscope (SEM, Model JSM-5900, JEP, Tokyo, Japan). The average grain sizes were measured from the micrographs and calculated by the SMile-View software. The oxide ionic conductivity of the materials was measured using electrochemical impedance spectroscopy based on sintered pellets. Both sides of the pellets were coated with silver paste as electrodes and fired at 700 °C for 10 min before measurement to ensure good bonding. The pellets were mounted in an alumina supporter and jigged with Pt wires using ceramic springs. The AC impedance spectra of the pellets were measured in the range of 200–500 °C in air using an impedance analyzer (PARSTAT 2273) over 0.1 Hz–100 kHz. Curve fitting and resistance calculations were carried out using ZSimpWin software.

3. Results and discussion

3.1. Synthesis characterization

Fig. 1 shows the XRD patterns of the specimens. As can be seen in Fig. 1(a), after calcining in air at 1200 °C for 2 h, although a slight Y_2O_3 peak is found in CeO_2–Y_2O_3 system, all the samples show corresponding crystalline fluorite single-phase. For the samples with ZnO additive (sintered at 1400 °C for 10 h), the XRD patterns show a pure cubic structure without any second phases (Fig. 1(b)).

Table 2 lists the values of sintering temperatures, soaking times, relative densities and average grain sizes of the sintered specimens. The relative densities are above 95% for 20YDC and 20GDC samples sintered at different temperatures, with or without ZnO additive. 20SDC samples show lower relative densities (89–94%). The results shown in Table 2 thus confirm that the addition of ZnO has beneficial effect on the sintering of ceria-based powder compacts, which are in agreement with previous reported results [7,8]. The rapid densification of ZnO-added specimens may be attributed to a viscous flow sintering mechanism, which increases the contact area of particles in a compact solid. It is noted that lower sintering temperature (1400 °C) and smaller grain sizes are obtained by ZnO doping. After sintering at 1600 °C for 10 h, the average grain sizes of ZnO added samples are about twice larger than those without ZnO.

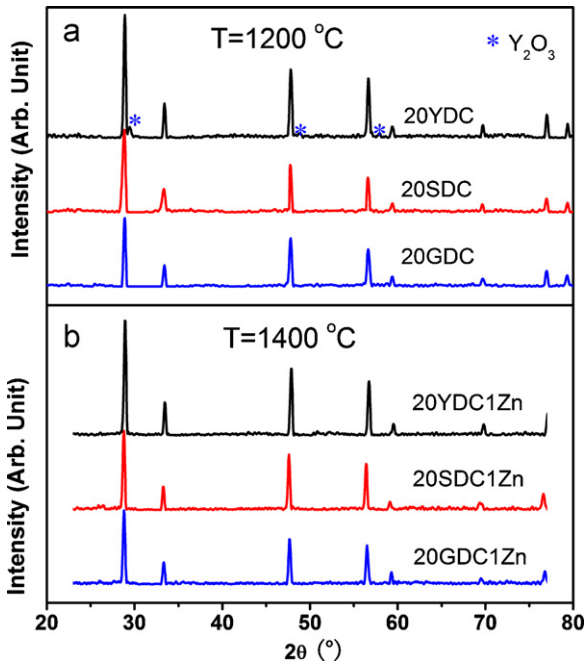

Fig. 1. X-ray patterns of 20YDC, 20GDC and 20SDC powders heated at 1200 °C for 2 h (a) and at 1400 °C for 10 h with ZnO additive (b).

3.2. Microstructure analysis

Fig. 2 shows a matrix of 9 SEM photographs which were taken from the surfaces of as-sintered samples. Of the samples, some present very special surface "island structures", as can be seen in Fig. 2(a), (d) and (g)–(i). The energy dispersive spectroscopy (EDS) results show the specific composition ratio of those second phases (Fig. 3). In particular, amorphous phase containing high amount of Y has been observed on all 20YDC samples sintered at different temperatures, with addition of ZnO or without (Fig. 3(I)–(IV)). This indicates that Y is prone to segregate at grain boundaries, compared to Sm and Gd.

Surprisingly, high level of Si has been identified on some samples. It is worthy to mention that the second phases appeared on ZnO-doped samples contain a considerable amount of Si and a little Ca, while this phenomenon was not observed on undoped samples after the same sintering condition. In other words, the addition of ZnO promotes the grain growth significantly (Table 2) and induces the enrichment of insulated impurities (e.g. Si) effectively.

Table 2
Relative density and average grain sizes of the ceria-based ceramics doped with 1 mol% ZnO (sintered at 1400 °C and 1600 °C) and without (sintered at 1600 °C).

Samples	Sintering T (°C)	Relative density (%)	Average grain size (μm)
20YDC	1600	95.4	3.099
20SDC	1600	89.2	2.502
20GDC	1600	96.7	4.446
20YDC1Zn	1400	96.2	2.085
20SDC1Zn	1400	91.6	1.865
20GDC1Zn	1400	96.5	3.051
20YDC1Zn	1600	97.2	5.492
20SDC1Zn	1600	93.4	4.764
20GDC1Zn	1600	96.5	9.527

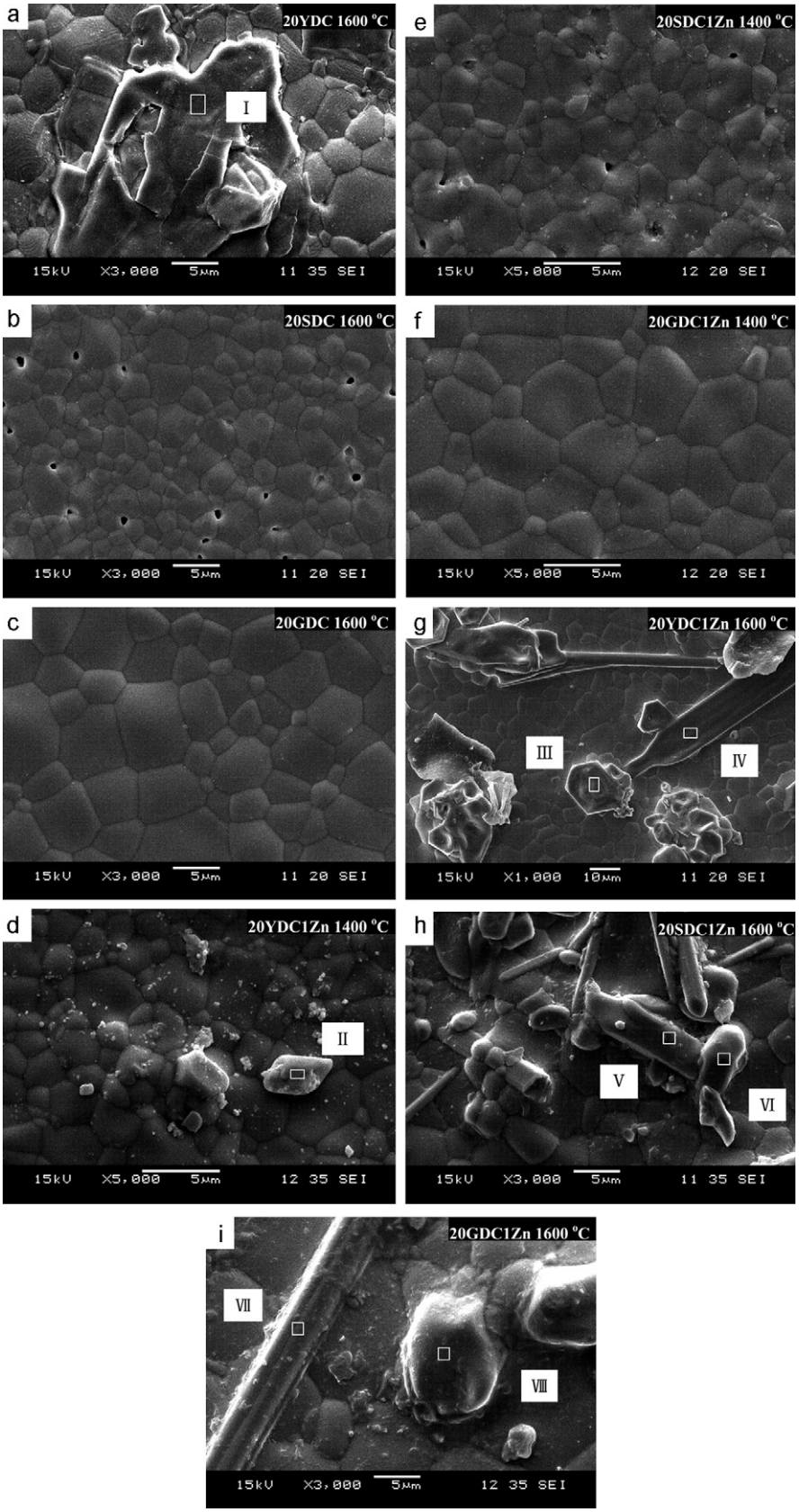

Fig. 2. Matrix of SEM photographs: (a) 20YDC, (b) 20SDC and (c) 20GDC sintered at 1600 °C for 10 h; (d) 20YDC + 1 mol% ZnO, (e) 20SDC + 1 mol% ZnO and (f) 20GDC + 1 mol% ZnO sintered at 1400 °C for 10 h; (g) 20YDC + 1 mol% ZnO, (h) 20SDC + 1 mol% ZnO and (i) 20GDC + 1 mol% ZnO sintered at 1600 °C for 10 h.

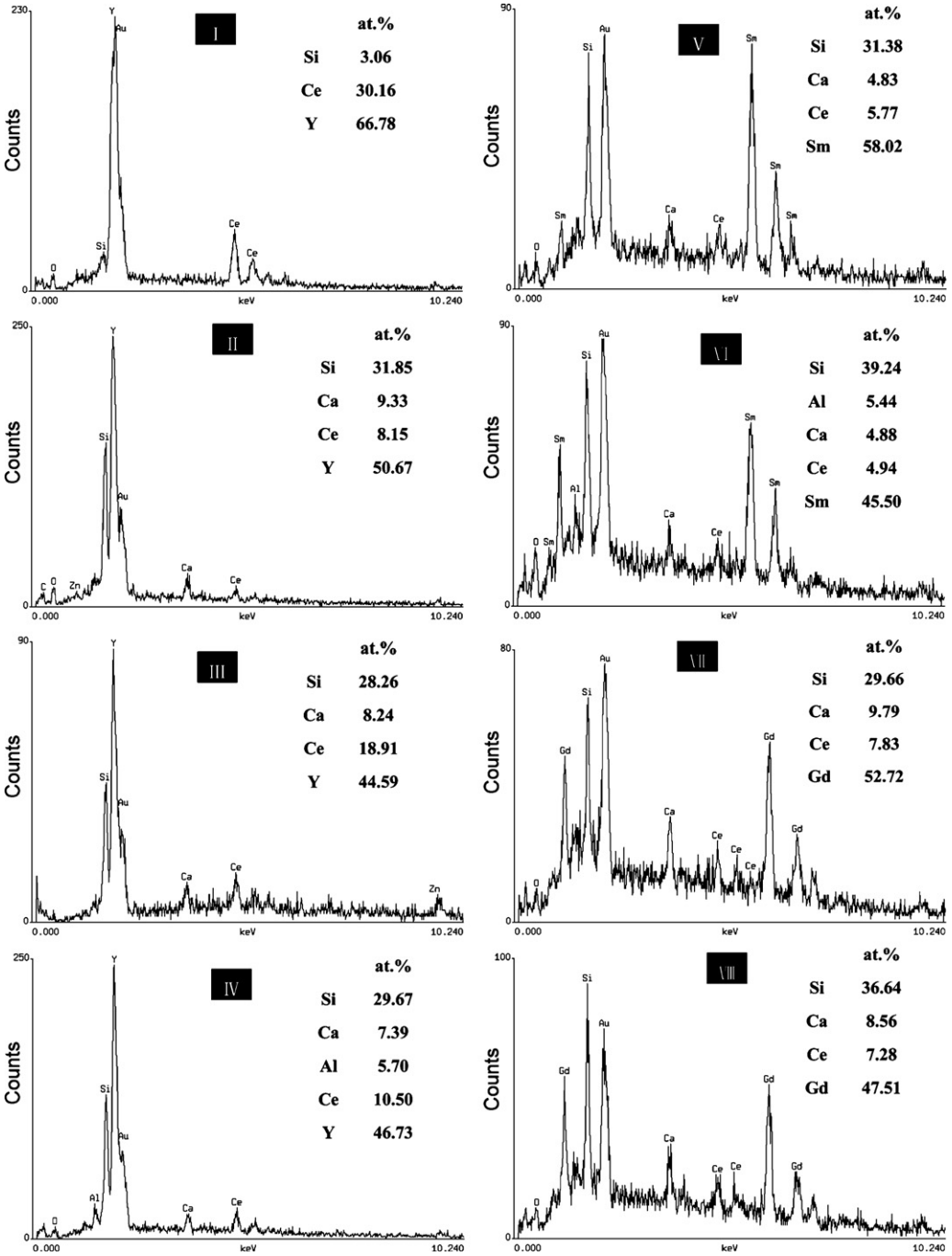

Fig. 3. EDS results of the specific areas marked in the SEM photographs. The numbers of the EDS photographs correspond to the numbers marked in the SEM photographs.

3.3. Impedance measurements

Fig. 4 shows the complex impedance spectra of the 20LnDC and 20LnDC1Zn specimens. The impedance spectra were curve fitted on assuming a series association of (RQ) terms, where R is the resistance and Q is a pseudo-capacitance. Generally, the relaxation time for the oxygen ion transfer through grain interior, grain boundary and electrode is well separated, hence distinct arcs are expected for each process in the impedance plot [24]. In order of decreasing frequency the arcs correspond to grain interior, grain boundary and electrode properties in correlation with the relaxation times. Actually, most impedance spectra fail to show well-resolved arcs for both grain-interior and grain-boundary contributions, which is mainly because of the limited frequency range of equipment and temperament dependence of grain interior and grain boundary contributions. For example, in this work, the grain interior relaxation frequency exceeds the upper limit of the equipment at 353 °C and the impedance spectra show only two arcs (Fig. 4). Fortunately, due to much higher capacitance values, the relaxation frequency of the grain boundary contribution is significantly lower at identical temperatures, which often allows fitting up to the temperature of 500 °C. Therefore, the grain boundary resistance can be calculated relatively accurate.

As can be seen in Fig. 4(a), the grain boundary resistance data (R_{gb}) were calculated and then subtracted these values from the total resistances to estimate the grain interior resistances ($R_{gi} \approx R_T - R_{gb}$). The obtained resistance R_{gi} was thus used to get the grain interior conductivity (Fig. 5) from the

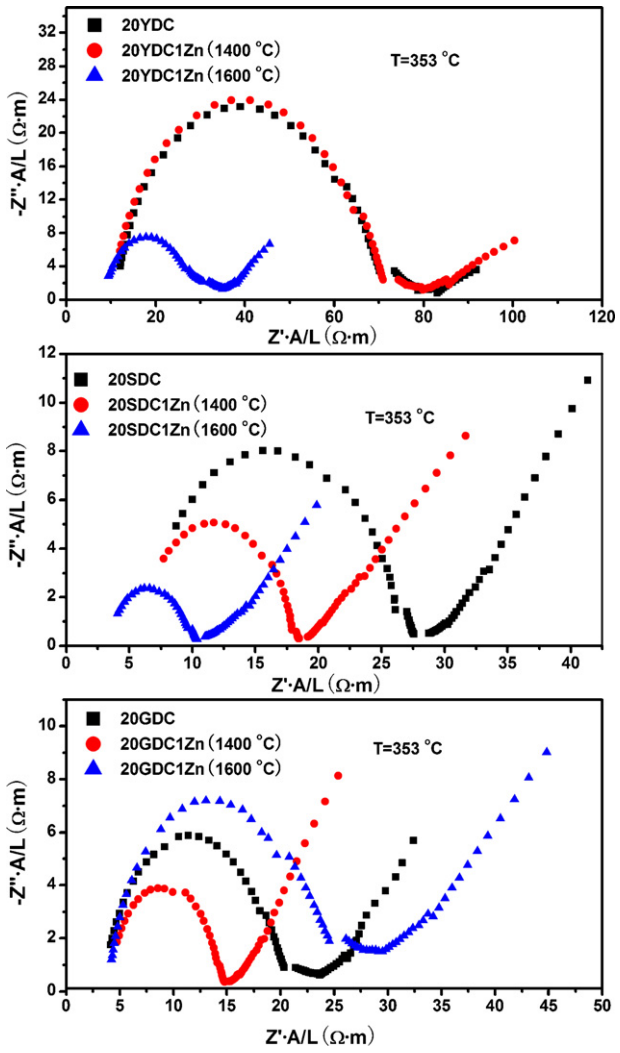

Fig. 4. Nyquist plots of impedance spectra obtained at 353 °C for ■ 20LnDC (sintered at 1600 °C for 10 h); ● 20LnDC1Zn (sintered at 1400 °C for 10 h); ▲ 20LnDC1Zn (sintered at 1600 °C for 10 h).

equation:

$$\sigma = \frac{1}{R} \times \frac{L}{A} \quad (1)$$

where L is the separation of the electrodes (usually the sample thickness) and A is the electrode area.

3.4. Grain interior transport properties

Fig. 5(a) shows that the addition of ZnO causes only a minor perturbation in σ_{gi}, which is in agreement with the previous reports on CoO, MgO and Fe_2O_3 doped ceria-based electrolytes [11,22,23]. It is interesting to note that, the 20YDC1Zn and 20SDC1Zn samples sintered at elevated temperature (1600 °C) show increased σ_{gi} (Fig. 5(b)). According to previous reports [15,25,26], whether the exact effect of increasing grain size on σ_{gi} beneficial or detrimental is still debated, while this effect was considered very limited. Thus the enhancement might suggest the effect of ZnO on σ_{gi} is remarkable. These changes might be due to temperature dependence of solubility of Zn and the defect association. Excess oxygen vacancies are generated as the Ce^{4+} is replaced by Zn^{2+} cation, the reaction can be expressed as:

$$ZnO \xrightarrow{CeO_2} Zn''_{Ce} + O_O^{\times} + V_O^{\bullet\bullet} \quad (2)$$

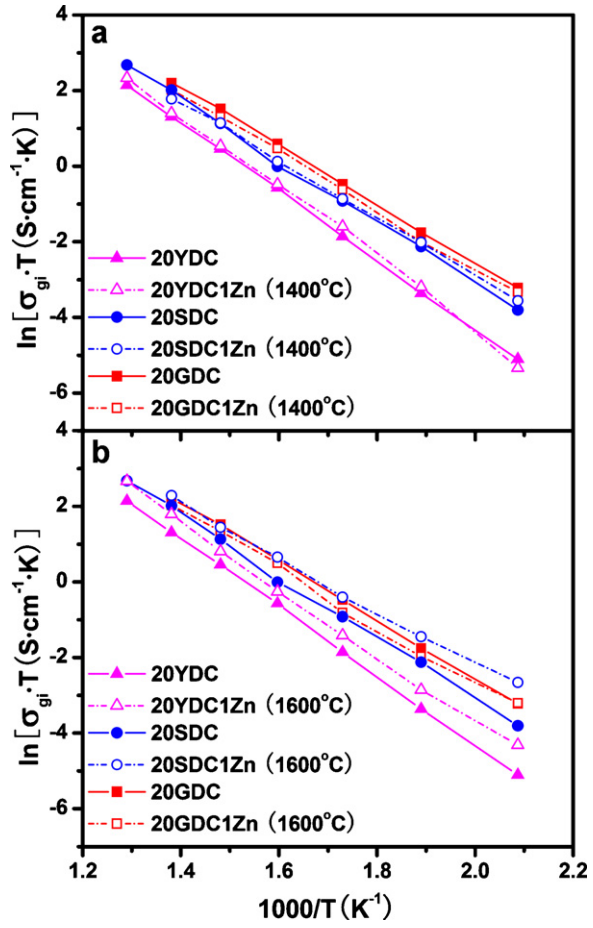

Fig. 5. Grain interior conductivity of 20LnDC and 20LnDC1Zn. The 20LnDC1Zn samples were, respectively, sintered at (a) 1400 °C and (b) 1600 °C for 10 h. 20LnDC were sintered at 1600 °C for 10 h.

The formation of $V_O^{\bullet\bullet}$ would increase the σ_{gi}, but the defect association effect between $V_O^{\bullet\bullet}$ and Zn''_{Ce} or Ln'_{Ce} would decrease the σ_{gi} [27,28]. The effect of ZnO being either beneficial or detrimental to the grain interior conductivity depends on the sintering temperatures and materials compositions.

3.5. Grain boundary behaviour

Fig. 4 also shows that the addition of ZnO can improve the grain boundary behaviours of ceria-based electrolytes. A lower grain boundary resistance was obtained when 20YDC1Zn and 20SDC1Zn samples sintered at 1600 °C; 20GDC1Zn samples sintered at 1400 °C.

The series grain boundary conductivity calculated from Eq. (1) with the appropriate R_{gb} is the apparent grain boundary conductivity σ_{gb}^{app} (Fig. 6), as it is calculated with R_{gb} and the macroscopic dimension of the sample (thickness/area) [15]. As shown in Fig. 6, with ZnO doping, the values of σ_{gb}^{app} can be improved significantly via sintering at certain temperatures. In particular, the samples of 20YDC1Zn sintered at 1600 °C exhibit huge increases in σ_{gb}^{app}; the 20SDC1Zn samples show considerable improved σ_{gb}^{app}, whatever sintered at 1400 °C or 1600 °C; the 20GDC1Zn samples sintered at 1400 °C indicate increased σ_{gb}^{app} but those sintered at 1600 °C on the contrary.

As good sintering aids for ceria ceramics, the effects of many transition metal oxides (TMOs) on the grain boundary conductivity have been studied and well documented [19–23]. Zhang et al. found

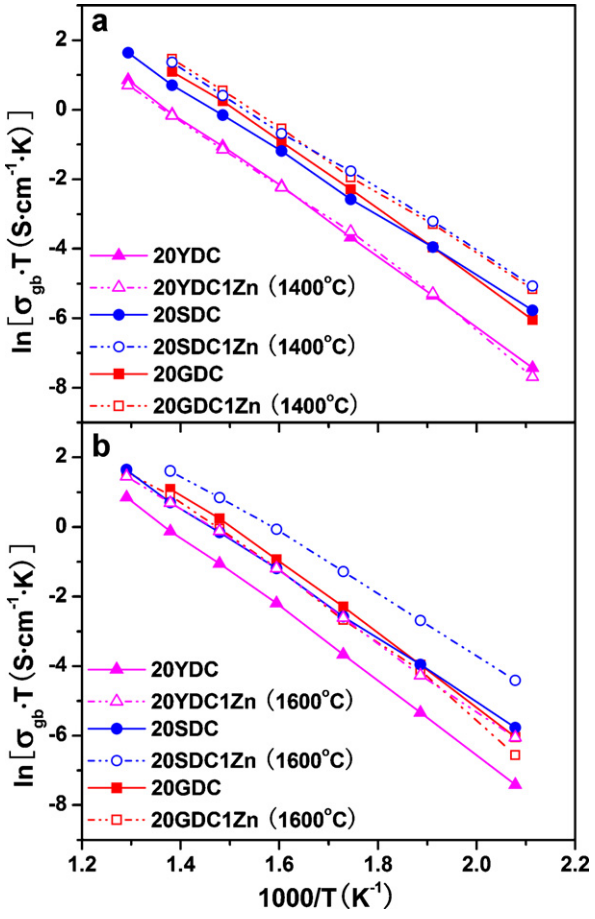

Fig. 6. Apparent grain boundary conductivity of 20LnDC and 20LnDC1Zn. The 20LnDC1Zn samples were, respectively, sintered at (a) 1400 °C and (b) 1600 °C for 10 h. 20LnDC samples were sintered at 1600 °C for 10 h.

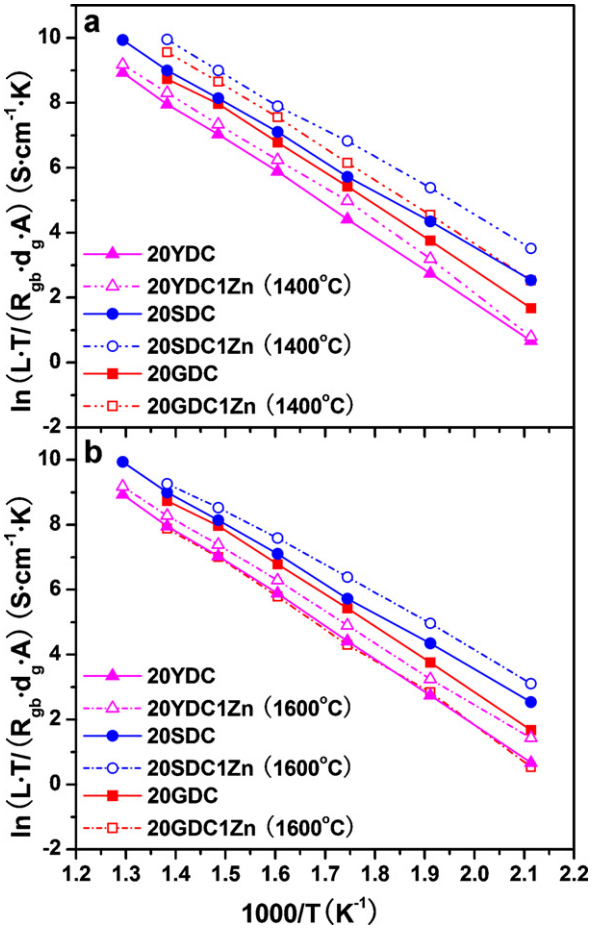

Fig. 7. Alternative representation of the specific grain boundary conductivity of 20LnDC and 20LnDC1Zn. The 20LnDC1Zn samples were, respectively, sintered at (a) 1400 °C and (b) 1600 °C for 10 h. 20LnDC samples were sintered at 1600 °C for 10 h.

that Co_2O_3 or MnO_2 doping has detrimental effect on grain boundary behaviour of 20GDC, especially for Si-containing samples, while the addition of Fe_2O_3 has scavenging effect on SiO_2 impurity and improves the grain boundary conduction significantly [19]. Cho and his colleagues investigated the effect of MgO and CaO on the grain-boundary conduction of 10GDC, respectively [22,29]. They found that small amount of MgO or CaO doping can enhance the grain-boundary conduction of 500-ppm-SiO_2-doped 10GDC by tens of times. In this study, the exact content of SiO_2 is unavailable. Nevertheless, the results in Figs. 4 and 6 clearly show that the apparent grain boundary conduction of 20LnDC is enhanced obviously by the addition of 1 mol% ZnO.

The σ_{gb}^{app} value is calculated from the dimensions of the electrode area and sample thickness, not from the geometry of the grain-boundaries. Thus, in order to investigate the true changes in grain boundary behaviours, the specific grain-boundary conductivity (σ_{gb}^{sp}) should be estimated from the geometry of the grain boundary.

A brick-layer model has been employed extensively to correlate the microstructure with the grain and grain-boundary conduction behaviours and explain the variation of ionic conductivity as a function of grain size [15,18,24,26,30]. This model was proposed by Van Dijk and Burggraaf [31], assumes that the ceramic samples consist of highly conducting grains, separated by continuous and uniform grain boundary layers. Assuming that all the grains are cubic with equal size of d_g, separated by flat grain boundaries of thickness δ_{gb} where $\delta_{gb} \ll d_g$. Then the specific grain-boundary conductivity (σ_{gb}^{sp}) can be estimated by the following equation [15,18,26]:

$$\sigma_{gb}^{sp} = \sigma^{app}\frac{\delta_{gb}}{d_g} = \frac{1}{R_{gb}} \times \frac{L}{A} \times \frac{\delta_{gb}}{d_g} \quad (3)$$

Actually, the typical values of grain boundary thickness change in a relatively narrow range for all samples with different trivalent additives, and with or without sintering aid [11]. Thus, in some way, the changes in $L/(R_{gb}d_gA)$ can represent the true changes in grain boundary behaviours. Similar approximate treatment was adopted to assess the specific grain-boundary behaviour of polycrystalline samples in previous reports [26,27].

Fig. 7(a) suggests that the σ_{gb}^{sp} of 20LnDC1Zn (sintered at 1400 °C) are much higher than that of 20LnDC. According to brick-layer model, σ_{gb}^{sp} would increase with the decrease of grain sizes, as reducing the Si concentration low enough to vary the grain-boundary coverage of silicon. Thus, the enhancement of the σ_{gb}^{sp} shown in Fig. 7(a) may be due in large part to the decrease of the average grain size (Table 2).

Even more noteworthy is that Fig. 7(b) also shows remarkable improvement in σ_{gb}^{sp} for 20YDC1Zn and 20SDC1Zn (sintered at 1600 °C) versus 20YDC and 20SDC, respectively. Considering the fact that the ZnO-added samples corresponded to Fig. 7(b) have larger grain sizes (Table 2) and corresponding less numbers of grain boundaries, the enhancements shown in Fig. 7(b) are inconsistent with the brick layer model. Obviously, the addition of ZnO should be responsible for this paradoxical tendency. That point is supported by the results of SEM and EDS. Comparing the surface structures

of 20LnDC (Fig. 2(a)–(c)) and 20LnDC1Zn (sintered at 1600 °C) (Fig. 2(g)–(i)), enrichment of Si was observed on those ZnO-added samples (Fig. 3(III)–(VIII)) and this phenomenon is believed to be associated with the enhancement of σ_{gb}^{sp} in Fig. 7(b). Puzzlingly, Zn element was not detected in the EDS results. Thus, the mechanism of Si-enrichment might not be simply explained by forming eutectic compounds between ZnO and impurities.

The decrease in σ_{gb}^{sp} for 20GDC1Zn samples in Fig. 7(b) may be attributed to their outstanding grain sizes (average 9.527 μm). As the grain size of 20GDC1Zn (sintered at 1600 °C) is much larger than other samples (Table 2), although plenty of impurities were trapped on the surfaces, the concentration of the insulated phase at the grain boundaries is high enough to decrease the σ_{gb}^{sp}.

A parallel model was proposed by Schouler et al. [32] at 1973 and they suggested the grain boundaries are partially blocked, the ionic current across grain boundaries was considered to flow in two paths. On path of high resistance partially covers the grain boundaries, the other one is through the clean grain boundaries of grain–grain contact. As the resistivity from clean grain boundaries is much smaller than that from glassy phases, the overall grain boundary resistivity is determined mainly by the grain-to-grain contact region but not by the glassy phase [15]. In the present case, the parallel model may give a better explanation of the grain boundary behaviours. As the grain boundary area is so large that the finite amount of impurities contained in these samples are not sufficient to form a continuous glassy phase layer along grain boundaries. Thus the grain-to-grain contact becomes the dominate pathway of ion transfer and the ZnO added samples (sintered at 1400 °C) consequently exhibit higher grain boundary conductivity. For 20LnDC1Zn samples (sintered at 1600 °C), as ZnO-doping induced the enrichment of insulated phases on the surfaces of samples, the remaining grain boundary areas can still contain clean grain-to-grain contact and the specific grain boundary conductivities remain corresponding high values.

Other factors might also affect the grain boundary conductivity, such as space charge effects, dopant segregation behaviours and the level of contamination by impurities (e.g. silica). In addition, the mechanisms of ZnO scavenging effect have not been established yet. These issues will be dealt in a future work.

4. Conclusions

The addition of 1 mol% zinc oxides promotes the densification and grain growth of doped ceria considerably. The effect of ZnO additive on the grain interior conductivity cannot be ignored when sintered at elevated temperature (1600 °C). The addition of ZnO significantly increases both the apparent and specific grain boundary conductivities. Si-enrichment observed on the surfaces of ZnO added samples might be the reason of the enhanced grain boundary conductions. In summary, for ceria-based electrolytes, ZnO not only is a good sintering aid for densification but also acts as effective grain boundary scavenger. Although the mechanisms of ZnO scavenging effect have not been established yet, this finding is believed to be advantageous in improving the performance of ceria-based electrolytes.

Acknowledgement

A Project Funded by the Priority Academic Program Development (PAPD) of Jiangsu Higher Education Institutions. We also acknowledge the support of Jiangsu Provincial Key Laboratory of Inorganic and Composite Materials.

References

[1] D.J.L. Berett, A. Atkinson, N.P. Brandon, S.J. Skinner, Chem. Soc. Rev. 37 (2008) 1568–1578.
[2] T. Kudo, H. Obayashi, J. Electrochem. Soc. 122 (1975) 142–147.
[3] H. Yahiro, K. Eguchi, H. Arai, Solid State Ionics 36 (1989) 71–75.
[4] D.Y. Wang, A.S. Nowick, J. Solid State Chem. 35 (1980) 325–333.
[5] H. Yoshida, K. Miura, T. Fukui, S. Ohara, T. Inagaki, J. Power Sources 106 (2002) 136–141.
[6] Y. Zheng, C. Chen, S. Li, L. Ge, H. Chen, L. Guo, Mater. Res. Bull 46 (2011) 130–135.
[7] L. Gao, M. Zhou, Y. Zheng, H. Gu, H. Chen, L. Guo, J. Power Sources 195 (2010) 3130–3134.
[8] S. Li, L. Ge, H. Gu, Y. Zheng, H. Chen, L. Guo, J. Alloys Compd. 509 (2011) 94–98.
[9] H. Inaba, H. Tagawa, Solid State Ionics 83 (1996) 1–16.
[10] K. Eguchi, T. Setoguchi, T. Inoue, H. Arai, Solid State Ionics 52 (1992) 165–172.
[11] D. Pérez-Coll, D. Marrero-López, P. Núñez, S. Piñol, J.R. Frade, Electrochim. Acta 51 (2006) 6463–6469.
[12] B.C.H. Steele, Solid State Ionics 129 (2000) 95–110.
[13] X. Guo, W. Sigle, J. Maier, J. Am. Ceram. Soc. 86 (2003) 77–78.
[14] M.J. Verkerk, B.J. Middelhuis, A.J. Burggraaf, Solid State Ionics 6 (1982) 159–170.
[15] C. Tian, S.W. Chan, Solid State Ionics 134 (2000) 89–102.
[16] R. Gerhardt, A.S. Nowick, J. Am. Ceram. Soc. 69 (1986) 641–646.
[17] R. Gerhardt, A.S. Nowick, M.E. Mochel, I. Dumler, J. Am. Ceram. Soc. 69 (1986) 647–651.
[18] S. Hui, J. Roller, S. Yick, X. Zhang, C. Decès-Petit, Y. Xie, R. Maric, D. Ghosh, J. Power Sources 172 (2007) 493–502.
[19] T.S. Zhang, J. Ma, Y.J. Leng, S.H. Chan, P. Hing, J.A. Kilner, Solid State Ionics 168 (2004) 187–195.
[20] X. Zhang, C. Decès-Petit, S. Yick, M. Robertson, O. Kesler, R. Maric, D. Ghosh, J. Power Sources 162 (2006) 480–485.
[21] H. Yoshida, T. Inagaki, J. Alloys Compd. 408–412 (2006) 632–636.
[22] Y.H. Cho, P.S. Cho, G. Auchterlonie, D.K. Kim, J.H. Lee, D.Y. Kim, H.M. Park, J. Drennan, Acta Mater. 55 (2007) 4807–4815.
[23] T.S. Zhang, J. Ma, L.B. Kong, S.H. Chan, P. Hing, J.A. Kilner, Solid State Ionics 167 (2004) 203–207.
[24] H.L. Tuller, Solid State Ionics 131 (2000) 143–157.
[25] R.K. Lenka, T. Mahata, A.K. Tyagi, P.K. Sinha, Solid State Ionics 181 (2010) 262–267.
[26] G.M. Christie, F.P.F. van Berkel, Solid State Ionics 83 (1996) 17–27.
[27] M. Mogensen, N.M. Sammes, G.A. Tompsett, Solid State Ionics 129 (2000) 63–94.
[28] J.A. Kilner, Solid State Ionics 129 (2000) 13–23.
[29] P.S. Cho, S.B. Lee, Y.H. Cho, D.Y. Kim, H.M. Park, J.H. Lee, J. Power Sources 183 (2008) 518–523.
[30] J. Maier, Ber. Bunsenges. Phys. Chem 90 (1986) 26–33.
[31] T. Van Dijk, A.J. Burggraaf, Phys. Status Solidi (a) 63 (1981) 229–240.
[32] E. Schouler, G. Girond, M. Kleitz, J. Chem. Phys. 70 (1973) 1309–1315.